

Quantum Monte Carlo study of an anharmonic Holstein model

G. Paleari,^{1,2} F. Hébert,^{1,*} B. Cohen-Stead,³ K. Barros,⁴ R.T. Scalettar,³ and G.G. Batrouni^{1,5,6,7}

¹*Université Côte d'Azur, CNRS, INPHYNI, France*

²*Dipartimento di Fisica, Università degli Studi di Milano, via Celoria 16, 20133 Milano, Italy*

³*Department of Physics, University of California, Davis, California 95616, USA*

⁴*Theoretical Division and CNLS, Los Alamos National Laboratory, Los Alamos, New Mexico, 87545, USA*

⁵*Department of Physics, National University of Singapore, 2 Science Drive 3, 117542 Singapore*

⁶*Centre for Quantum Technologies, National University of Singapore; 2 Science Drive 3 Singapore 117542*

⁷*Beijing Computational Science Research Center, Beijing 100193, China*

We study the effects of anharmonicity on the physics of the Holstein model, which describes the coupling of itinerant fermions and localized quantum phonons, by introducing a quartic term in the phonon potential energy. We find that the presence of this anharmonic term reduces the extent of the charge density wave phase (CDW) at half-filling as well as the transition temperature to this phase. Doping away from half-filling, we observe a first order phase transition between the CDW and a homogeneous phase which is also present in the harmonic model. In addition, we study the evolution of the superconducting susceptibility in the doped region and show that anharmonicity can enhance the superconducting response.

PACS numbers: 71.10.Hf, 71.30.+h, 71.45.Lr, 63.20.-e

I. INTRODUCTION

Electron-phonon interactions in solids drive a number of quantum many body effects. One is conventional superconductivity (SC).^{1,2} Another is the formation of insulating charge density wave (CDW) phases.³⁻⁵ Complex Hamiltonians which describe both many electronic orbitals and multiple phonon bands, are typically needed to describe these phenomena in real materials. Fortunately, simplified models can often capture the key qualitative consequences of the electron-phonon coupling, while being much more analytically and computationally tractable.

The Holstein Hamiltonian⁶ is one such model. It describes a single electronic band and dispersionless quantum phonons coupled locally to the fermion density. A considerable body of computational work exists for the Holstein model. Studies of the dilute limit reveal how individual electrons are dressed by phonons, and the effective mass and transport properties of these ‘polarons’ have been evaluated.⁷⁻¹⁵ At higher densities, the emergence of SC at generic fillings, and gapped CDW phases at commensurate occupations has been investigated.¹⁶⁻²³

The solution of even this relatively simple model is not, however, computationally easy. Only relatively recently have the critical temperatures for the CDW transition been evaluated for the square²⁴ and cubic²⁵ lattices via quantum Monte Carlo (QMC). Likewise, the determination of the critical interaction strength at the quantum critical point for the CDW transition on a honeycomb lattice is a rather new development.²⁶ Analytic approaches, especially Migdal-Eliashberg theory^{27,28} have been critical to the understanding of the Holstein Hamiltonian.^{29,30} Their comparison with QMC has been an especially useful line of investigation, especially in efforts to determine the

largest possible SC transition temperature.³¹

In the course of these studies, it has become apparent that the Holstein Hamiltonian has a significant deficiency in some parameter regimes. Specifically, it has been shown³² that the values of the phonon displacement reached in CDW phases could be quite large, even reaching values comparable to the intersite spacing in the system. Thus, the harmonic description of phononic excitations in the medium provided by the Holstein model may not be sufficient, and the effects of anharmonic terms on the phases of Holstein systems should be taken into account.^{32-37,39-41} Several approaches to include anharmonic effects have been considered, for example nonlinear coupling terms between fermions and phonons,³²⁻³⁷ or quartic³⁸⁻⁴⁰ or Gaussian⁴¹ contributions to the phonon potential energy. Anharmonicity has also been considered in the context of Migdal-Eliashberg theory.⁴²⁻⁴⁴

In infinite dimension, using a technique similar to dynamical mean field theory (DMFT), Freericks, Jarrell, and Mahan⁴⁰ studied the effects of a simple anharmonic term in the form of an additional quartic potential energy for the phonons. They concluded that a CDW phase exists for a large range of densities at low anharmonicity, but that the CDW is gradually replaced at low and high densities by a SC phase as the anharmonicity increases. The half-filled system always remains in a CDW state. They also observed a decrease of the critical temperatures at which CDW and SC phases appear with increasing anharmonicity. Similar models have been studied in one dimension.³⁹

The goal of this article is to study the effects of such an additional quartic anharmonic term on the behavior of the Holstein model in two dimensions using a recently introduced Langevin algorithm.^{45,46} Unlike DMFT, the Langevin approach handles spatial correlations in finite dimensions without introducing systematic error. In

section III, we will introduce the Holstein model and its anharmonic extension, as well as the methods we will use to study the system and characterize the different phases. Section II will be devoted to the study of the behavior at half-filling, especially the CDW phase and how it evolves with anharmonicity. Section IV will concentrate on the behavior away from half-filling, discussing possible CDW phases as well as superconducting behavior. We will then give some final thoughts and conclusions.

II. MODEL AND METHODS

We study a generalized version of the Holstein Hamiltonian which incorporates anharmonicity in a specific way, namely as an additional term in the quantum phonon potential energy:⁴⁰

$$H - \mu N = -t \sum_{\langle ij \rangle \sigma} (c_{i\sigma}^\dagger c_{j\sigma} + h.c.) - \mu \sum_{i\sigma} n_{i\sigma} \quad (1)$$

$$+ \sum_i \left(\frac{m\omega^2 x_i^2}{2} + \frac{p_i^2}{2m} \right) + \omega_4 \sum_i x_i^4 \quad (2)$$

$$+ \lambda \sum_{i\sigma} x_i n_{i\sigma} \quad (3)$$

The sums run over the L^2 sites of a two-dimensional square lattice. The operator $c_{i\sigma}$ ($c_{i\sigma}^\dagger$) destroys (creates) a fermion of spin $\sigma = \uparrow$ or \downarrow on site i ; $n_{i\sigma} = c_{i\sigma}^\dagger c_{i\sigma}$ is the corresponding number operator; x_i and p_i are the canonical displacement and momentum operators of the phonon mode at site i . The first term (Eq. 1) represents the hopping energy of the fermions between neighboring sites $\langle ij \rangle$. A chemical potential term is included as our algorithm performs the simulations in the grand canonical ensemble. The hopping parameter t will be used as the energy scale. The second term (Eq. 2) represents the energy of the phonons of harmonic frequency ω and includes an anharmonic term proportional to x_i^4 with a prefactor ω_4 , and we put $m = 1$ in the rest of the article. The third term (Eq. 3) is the phonon-electron interaction. This coupling can be rewritten as $g \sum_{i\sigma} (a_i^\dagger + a_i) n_{i\sigma}$ where $g = \lambda/\sqrt{2\omega}$ and a_i and a_i^\dagger are the destruction and creation operators of phonons at site i . We focused on the cases where $g = 1$, $\omega = 0.5$ and $\omega = 1$. Using two values of ω yields the evolution of the anharmonic effects as a function of ω and also allows comparison with previous studies.^{40,52}

The average value of x_i on a doubly occupied site can be roughly estimated as $-2\lambda/\omega^2$ (see Appendix A). With this expression, the ratio η of the anharmonic to harmonic terms is given by

$$\eta \equiv \frac{16\omega_4 g^2}{\omega^5} \quad (4)$$

For $g = 1$ and $\omega < 1$, η becomes substantial even for relatively small values of ω_4 . Indeed, we will see that

$\omega_4 \lesssim 0.01$ is sufficient to affect profoundly the CDW physics at $\omega = 0.5$.

We study this model using a recently developed quantum Monte Carlo algorithm⁴⁵ based on a Langevin equation approach.⁴⁶ This method does not suffer from the sign problem for the Holstein model and the scaling of the simulation time with the number of sites is more advantageous than with conventional methods such as determinant quantum Monte Carlo (DQMC).⁴⁷ For the Langevin algorithm applied in two dimensions, the simulation time scales approximately as $L^{2.2}$ instead of L^6 for DQMC.⁴⁵ Throughout this work, we used sizes and inverse temperatures ranging up to $L = 16$ and $\beta = 20$, although, as will be seen, it is difficult to obtain reliable results for some quantities on large systems, especially away from half-filling or for small values of both ω and ω_4 .

The Langevin approach requires a discretization of the inverse temperature β . We used an imaginary time step $\Delta\beta = 0.1$ which we checked was sufficient so that systematic effects are smaller than statistical error bars. The Langevin time step was generally $dt = 10^{-3}$ and we used up to a few million Langevin steps for equilibration before performing measurements over up to 10^7 steps, using a standard binning of the data to analyze statistical errors.⁴⁸

We will look at the density $\rho = \sum_i \langle n_{i\sigma} \rangle / L^2$ and its behavior as a function of μ to detect the presence of charge gaps. We will also examine other simple diagonal quantities such as the average value of the phonon displacement $\langle x_i \rangle$ and the double occupancy $\langle n_{i\uparrow} n_{i\downarrow} \rangle$. In the harmonic case, the particle-hole symmetry yields an analytical expression for the chemical potential at half-filling $\mu = -\lambda^2/\omega^2$ and for the average value of the displacement $\langle x_i \rangle = -\lambda/\omega^2$ (see Appendix A). With $\omega_4 \neq 0$, there is no particle-hole symmetry and the value of μ for which the system is at half filling as well as the average displacement are unknown and must be determined by simulations, although some rough estimations can be made (App. A).

To characterize the presence of a CDW phase we study the charge structure factor, the Fourier transform at momentum (π, π) of the density-density correlation function,

$$S_{\text{cdw}} = \sum_i \langle n_i n_{i+j} \rangle (-1)^j. \quad (5)$$

Here n_i is the total number of particles on site i , $n_i = n_{i\uparrow} + n_{i\downarrow}$. The ordering vector for a half-filled square lattice is known to be at (π, π) . Incommensurate order at $q \neq (\pi, \pi)$ is possible upon doping, but we do not see evidence of it here. As the fermions enter the CDW phase, the electron-phonon coupling induces a corresponding order in the average values of $\langle x_i \rangle$ where $|\langle x_i \rangle|$ takes alternatively small and large values on neighboring sites, following the alternating values of the density n_i (see Fig. 1).

Away from half-filling, the system is suspected to

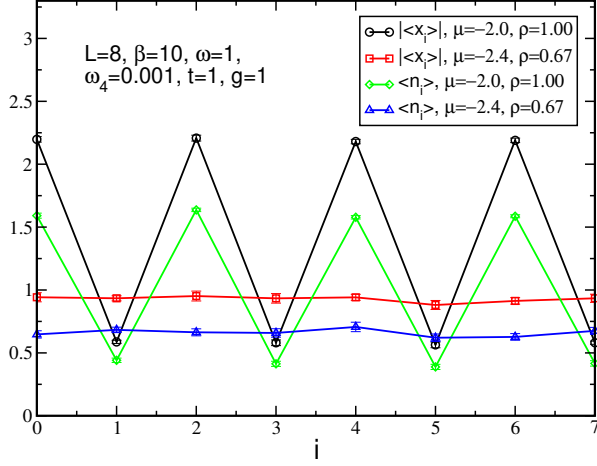


FIG. 1. Behavior of the average density, $\langle n_i \rangle$, and phonon displacement, $|\langle x_i \rangle|$, as functions of the position, i , along one axis in the square lattice in the homogeneous and CDW phases. In CDW phase at half-filling, there is symmetry breaking and two alternate values of $\langle n_i \rangle$ and $\langle x_i \rangle$ are observed. Out of half-filling, in an homogeneous phase, $\langle n_i \rangle$ and $\langle x_i \rangle$ are independent of the position.

be superconducting, with Cooper pairing driven by the phonons that generate on-site attraction U_{eff} between particles, as noted in the discussion of Eq. A3. We will look at this behavior through the s-wave pairing susceptibility

$$\chi_s = \frac{1}{L^2} \int_0^\beta d\tau \langle \Delta(\tau) \Delta^\dagger(0) + \text{h.c.} \rangle, \quad \Delta(\tau) = \sum_i c_{i\downarrow}(\tau) c_{i\uparrow}(\tau) \quad c_{i\sigma}(\tau) = e^{\tau H} c_{i\sigma} e^{-\tau H}. \quad (6)$$

III. HALF-FILLING

Without anharmonicity, the Holstein model develops a Peierls CDW phase at half-filling, where the chemical potential at half-filling is given by $\mu = -2g^2/\omega$. In the presence of the anharmonic term, however, we do not have an analytic expression for μ at half filling (App. A).

We first study the effects of the anharmonic term (Eq. 3) on this phase. To this end, we examine the evolution of the density as a function of μ at inverse temperature $\beta = 20$ which we verified had converged to the low temperature limit. A large system is not needed to obtain reliable measurements of the charge gap at half-filling, so we used $L = 6$. These simulations also determine the value of μ for which the system is at half-filling. We observe (Fig. 2) that ω_4 shifts the insulating plateau to larger values of μ and that the width of the half-filled density plateaux decrease with ω_4 . The other smaller plateaux that are observed away from half-filling

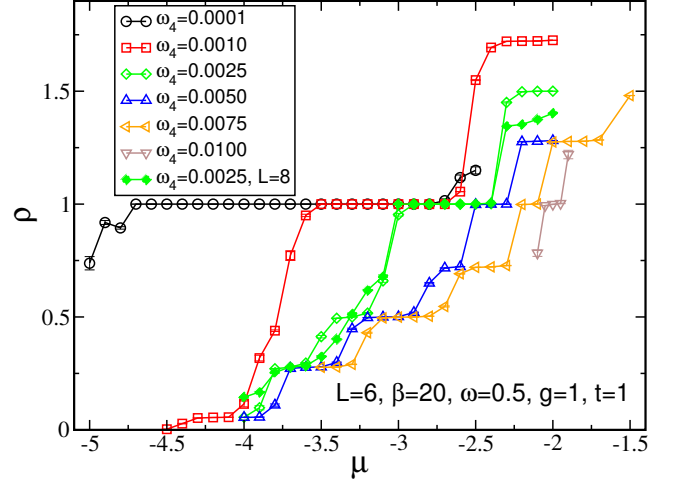


FIG. 2. (Color online). Density as a function of μ for different values of ω_4 . $L = 6, g = 1, \beta = 20, \omega = 0.5$. We find a reduction of the charge density gap found at half-filling when ω_4 is increased. The apparent gaps away from half filling are shell effects. A simulation at $L = 8, \omega_4 = 0.0025$ shows that half-filled plateau is not affected by finite size effects while the plateaux off of half-filling are reduced for larger sizes.

are finite size (‘shell’) effects due to the finite system size. These shell effects are revealed by nonzero ω_4 as it inhibits the CDW order. In Fig. 2, results from a $L = 8$ simulation for $\omega_4 = 0.0025$ show that these shell effects are reduced for larger sizes while the gap at half-filling remains essentially unchanged. This confirms that the small plateaux appearing off of half-filling are finite size effects, while the gap at half-filling is not.

The plateau at half-filling is a genuine collective effect, since there is no gap at half-filling at $g = 0$. Indeed, the density of states diverges there for a square lattice and only half of the states present at the Fermi level are occupied in the free system. Then, the gap observed at half-filling cannot be a spurious ‘shell’ effect, even on small size systems.

A collection of chemical potential sweeps such as that in Fig. 2, for different values of ω_4 , yields the boundaries of the CDW region in a phase diagram in the (μ, ω_4) plane. We delimit the CDW region with the value of μ for which $1 - \delta < \rho < 1 + \delta$, using a small threshold value δ . Figure 3 shows $\omega = 0.5$ in panel (a) and $\omega = 1$ in panel (b), for $\delta = 0.05$. The effect of ω_4 on the width and the position of the CDW gap is much stronger at $\omega = 0.5$ than at $\omega = 1$, as the ω dependence in expression for the relative size of the anharmonic term η in Eq. 4 would suggest should be the case. In both cases, we observe a shift of the chemical potential at half-filling towards smaller absolute values. This shift can be explained qualitatively using a simple approximation presented in Appendix A. The red triangles in Fig. 3 show the values of μ at $\rho = 1$ obtained with this approximation. In both cases, $\omega = 1$ and $\omega = 0.5$, we observe a reduction

of the charge gap (width of the CDW lobe) as ω_4 is increased although the effect is more dramatic for $\omega = 0.5$ (see Fig. 3 (c)). The sensitivity of the system to the anharmonic term in the $\omega = 0.5$ case is noticeable with strong differences already obtained for ω_4 of order 10^{-3} , a value for which $\eta \sim 0.5$. As the charge gap is much reduced for $\omega = 0.5$, it becomes smaller than the $\omega = 1$ charge gap as $\omega_4 \geq 0.0075$, despite the fact that it is much larger at small ω_4 (Fig. 3 (c)).

For large ω_4 , the gap becomes small in the $\omega = 0.5$ case (Fig. 3 (c)). We verified for larger systems that the small gap is not a finite size effect (Fig. 4). In these cases

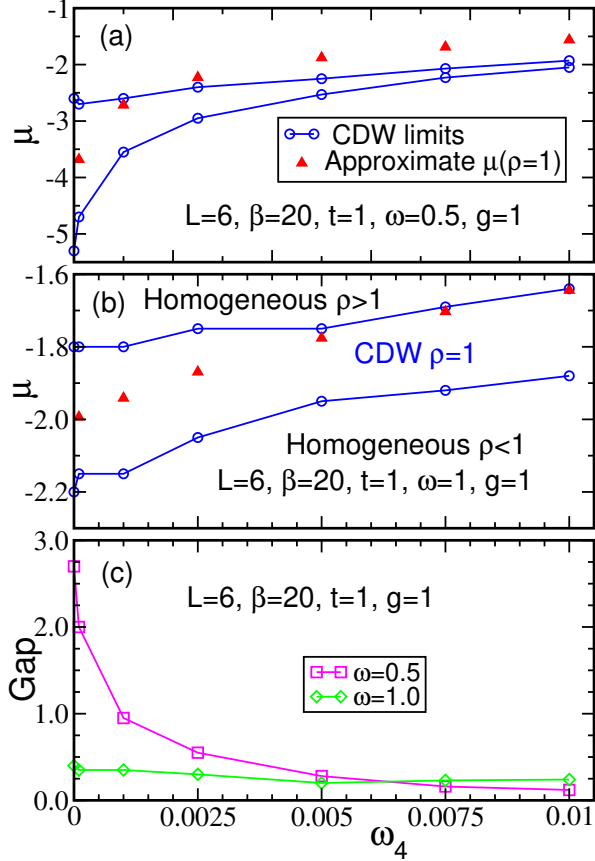


FIG. 3. (Color online). Phase diagrams of the system obtained from $L = 6$ simulations at $\beta = 20$ and $g = 1$, for $\omega = 0.5$ (a) and $\omega = 1$ (b) and comparison of the charge gaps in these cases (c). The anharmonic parameter ω_4 ranging from 0 to 0.01. The area enclosed by blue curves is the incompressible CDW phase at half-filling while the rest of the phase diagram corresponds to compressible phases that should become superconducting at low temperatures. The red triangles mark the half-filled chemical potential inferred from the approximate theory of Appendix A. The width of the CDW phase is strongly reduced due to the anharmonic effects for $\omega = 0.5$ (a). For $\omega = 1$ (b), the charge gap is relatively unaffected by the anharmonicity ω_4 in the range shown although it is generally smaller for $\omega = 1$ than for $\omega = 0.5$ (c).

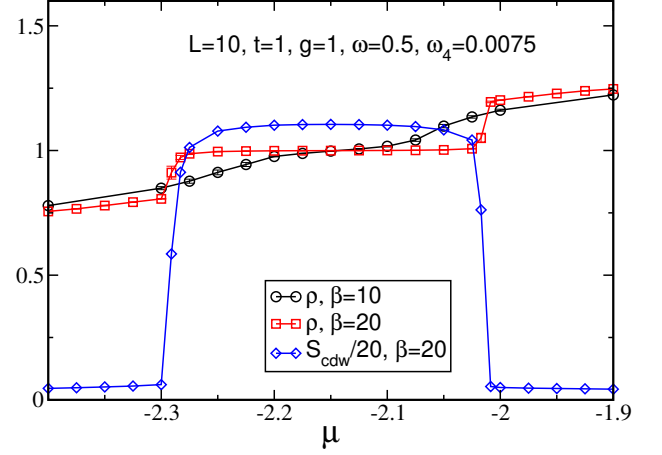


FIG. 4. (Color online). The density, ρ , and CDW structure factor, S_{cdw} , (rescaled for better visibility) for an $L = 10$ system, focusing on the CDW plateau. Notice that, for $\beta = 10$, the density does not yet show a plateau at half filling; $\beta = 20$ is necessary for the system to display the ground state behavior and exhibit the CDW gap. The structure factor S_{cdw} displays an abrupt change of values when the system is doped away from half-filling.

the plateau is rounded (Fig. 4) by thermal excitations at $\beta = 10$ and inverse temperatures up to $\beta = 20$ are needed to observe the flat plateau typical of the ground state behavior. We also observe an abrupt change of the density and of the CDW structure factor when the system is doped away from half-filling. In the parameter regime which is accessible to our QMC, we did not find a value for ω_4 where the gap at half-filling vanishes completely. The QMC simulations for $\omega_4 > 0.01$ become prohibitively difficult because they require exceedingly large values of β .

Knowing the values of μ where the system is half-filled, we performed several targeted simulations at half-filling. In Fig. 5 (top), we show the evolution of the average value $|\langle x_i \rangle| = -\langle x_i \rangle$ for different ω_4 and sizes, L , in the CDW phase at half-filling for the $\omega = 0.5$ case. We have not been able to obtain reliable results at this low temperature and large sizes for small values of ω_4 , the $\omega_4 = 0$ case being particularly difficult. We then compare to the analytical value at $\omega_4 = 0$, $|\langle x_i \rangle| = |-\lambda/\omega^2| = 4$ (see App. A). We find that, although it always extrapolates to a nonzero value, $|\langle x_i \rangle|$ is strongly reduced as ω_4 increases, by a factor of 2 at $\omega_4 = 0.01$ compared to $\omega_4 = 0$. This is expected as the anharmonicity penalizes large values of x , as does a large value of ω . As the phonon field generates an effective attraction between the fermions, this attraction is weakened and the double occupancy $\langle n_{i\uparrow} n_{i\downarrow} \rangle$ is correspondingly reduced, although it always remains larger than the uncorrelated value $\langle n_{i\uparrow} \rangle \langle n_{i\downarrow} \rangle$. This suppression of $|\langle x_i \rangle|$ and the resulting reduction of the effective attraction between fermions explain the observed shrinking of the CDW charge gap.

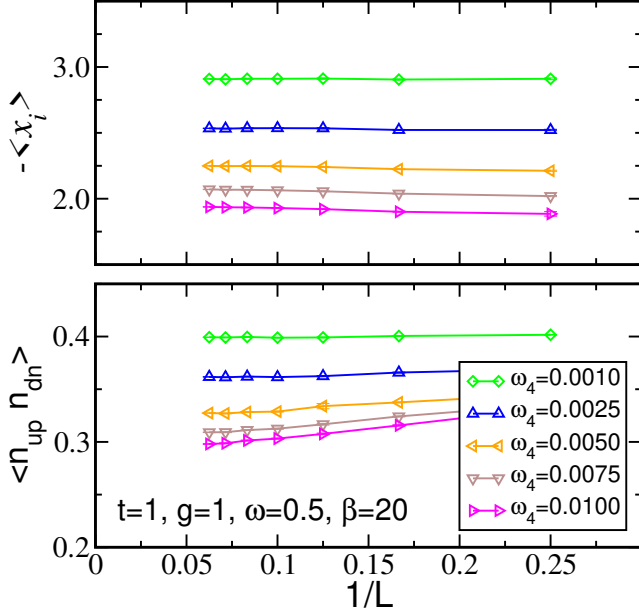


FIG. 5. (Color online). Average value $\langle x_i \rangle$ (top) and double occupancy (bottom) as functions of L^{-1} for different ω_4 in half-filled systems. $|\langle x_i \rangle|$ is reduced as ω_4 increases although it always extrapolates to nonzero values. For the harmonic case $\omega_4 = 0$, $\langle x_i \rangle = -4$. The double occupancy is also reduced but always extrapolates to values larger than $\langle n_{i\uparrow} \rangle \langle n_{i\downarrow} \rangle = 0.25$.

For $\omega = 1$, we find the same effects but with a much reduced amplitude. In that case, for $\omega_4 = 0$, $|\langle x_i \rangle| = \sqrt{2}$ which we have confirmed numerically (for $L = 16$ and $\beta = 20$, we find $|\langle x_i \rangle| = 1.4143(4)$). $|\langle x_i \rangle|$ varies from $\sqrt{2}$ down to $|\langle x_i \rangle| \simeq 1.3$ when ω_4 varies from 0 to 0.005 while $\langle n_{i\uparrow} n_{i\downarrow} \rangle$ decreases from $\langle n_{i\uparrow} n_{i\downarrow} \rangle \simeq 0.35$ to $\langle n_{i\uparrow} n_{i\downarrow} \rangle \simeq 0.33$ over the same ω_4 interval.

The gapped phase is expected to show CDW order, which we confirmed by a direct study of S_{cdw} at half-filling for different ω_4 (Fig. 6). In all the cases studied here, S_{cdw} extrapolates to a nonzero value in the thermodynamic limit $L \rightarrow \infty$ and is reduced as ω_4 increases. We verified the presence of a corresponding CDW order in the distribution of $|\langle x_i \rangle|$.

A. Finite temperature transition to CDW order

To complete this analysis of the CDW behavior at half-filling, we analyze the transition to this phase as the temperature, T , is lowered. The CDW transition breaks translation symmetry between the two sublattices of the square lattice. It is, therefore, in the universality class of the two-dimensional Ising model with a finite critical temperature, T_c , and 2D Ising critical exponents.

We used standard finite size scaling analysis where,

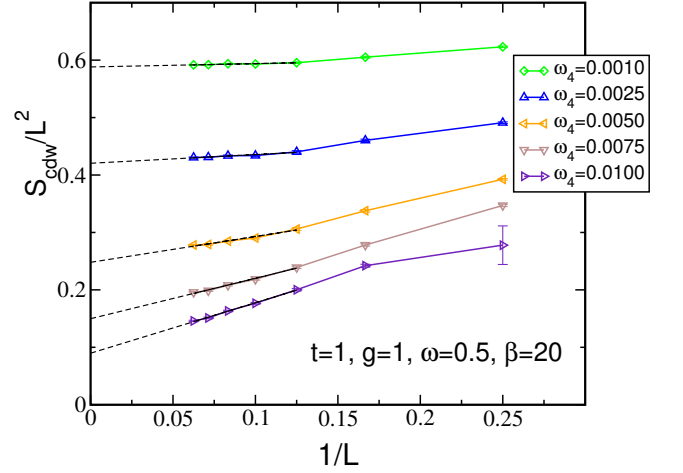


FIG. 6. (Color online). Structure factor S_{cdw} as a function of size L for different values of ω_4 at half-filling. For all ω_4 , the linear extrapolation of S_{cdw} to $L \rightarrow \infty$ is nonzero. The linear extrapolation is based on fits for the data with $L \geq 8$.

close to the transition, the structure factor behaves as

$$\frac{S_{\text{cdw}}}{L^2} = L^{-2\beta/\nu} \tilde{S}(L^{1/\nu} t) \Rightarrow S_{\text{cdw}} = L^{7/4} \tilde{S}(Lt), \quad (7)$$

with the critical exponents $\beta = 1/8$ and $\nu = 1$, $t = T - T_c$ is the reduced temperature, and \tilde{S} is a universal scaling function. As the critical exponents are known a priori, the only unknown quantity is T_c which will be chosen to optimize the superposition of the curves obtained for different system sizes (see Fig. 7). To do so, we choose a value of T_c , rescale all the data according to Eq. 7 and fit those data with a high degree polynomial. We then determine the optimal value of T_c as the one that minimizes the distance between the polynomial fit and the data. At large ω_4 , finite size corrections to scaling are larger and we have not found sizes where finite size scaling analysis can be used (see Appendix B), which limits the range in which we are able to determine the critical temperature.

As expected, T_c decreases with ω_4 (see Fig. 8). This behavior could have been inferred from the evolution of the charge gap and the structure factor at low temperatures. Compared to the infinite dimension results presented in Ref.[40], which focused on the $\omega = 0.5$ case, we observe a similar reduction of T_c with ω_4 . Our simulations show that the critical temperature changes from $T_c \simeq 0.25$ at $\omega_4 = 0$ down to $T_c \simeq 0.12$ at $\omega_4 = 0.005$. Freericks *et al.*⁴⁰ also predicted an initial increase of T_c with ω_4 . While we observe such an effect in some simulations, we cannot give a definite conclusion concerning this increase of T_c due to the lack of precision of our data for small ω_4 . The most remarkable difference with the infinite dimension description is the range of ω_4 over which noticeable changes are observed: we found a strong modification of critical temperature for $\omega_4 \simeq$

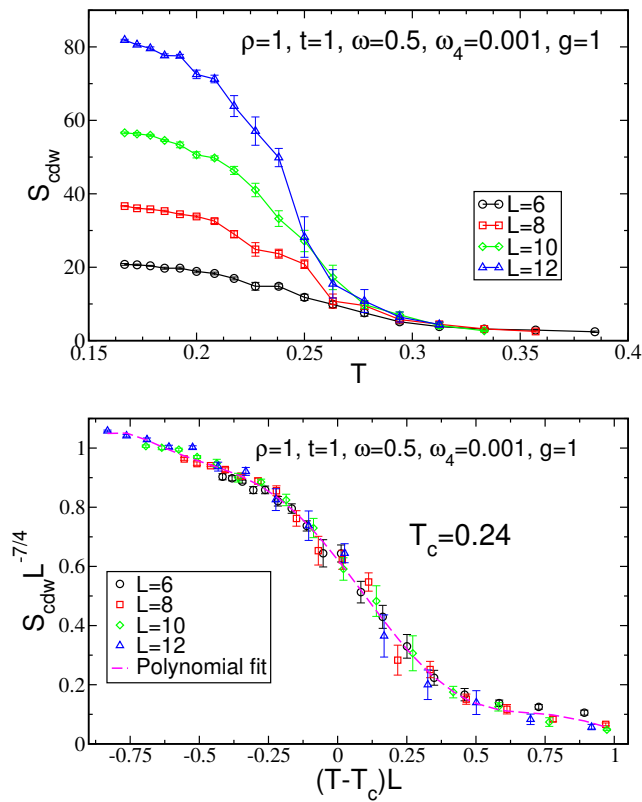


FIG. 7. (Color online). Finite size analysis for $\omega = 0.5$ and $\omega_4 = 0.001$. (Top) Structure factor for different sizes as a function of temperature T . (Bottom) Rescaled structure factor as a function of the rescaled reduced temperature. The critical temperature $T_c = 0.24 \pm 0.01$ is chosen to obtain the best possible collapse between the different curves.

$5 \cdot 10^{-3}$ whereas similar variations are found in⁴⁰ for $\omega_4 \simeq 10^{-1}$.

In the $\omega = 1$ case, for a similar range of ω_4 , we did not observe a strong change of the value of the critical temperature with ω_4 . Values of ω_4 where we could apply the finite size analysis were more restricted than for $\omega = 0.5$ and we could only get results for ω_4 up to 0.001. At $\omega_4 = 0$, we found a critical temperature of $T_c = 0.16 \pm 0.01$ which is compatible with values found recently in similar cases.^{24,49,50} For $\omega_4 = 0.001$ the critical temperature is barely reduced to $T_c = 0.15 \pm 0.01$. This was expected as we observed that, in this case, the anharmonicity hardly changes the width of the gap at half-filling.

Finally, for both $\omega = 0.5$ and $\omega = 1$, we observed a reduction of the charge gap and critical temperature as ω_4 increases but we did not observe a disappearance of the CDW phase in the accessible parameter range. For larger values of ω_4 , as in the pure Holstein case,²³ there are two possible scenarios. The first is a persistence of the CDW phase at half-filling with decreasing gap and critical temperature, which is possible because our model retains the Fermi surface nesting present in the Holstein

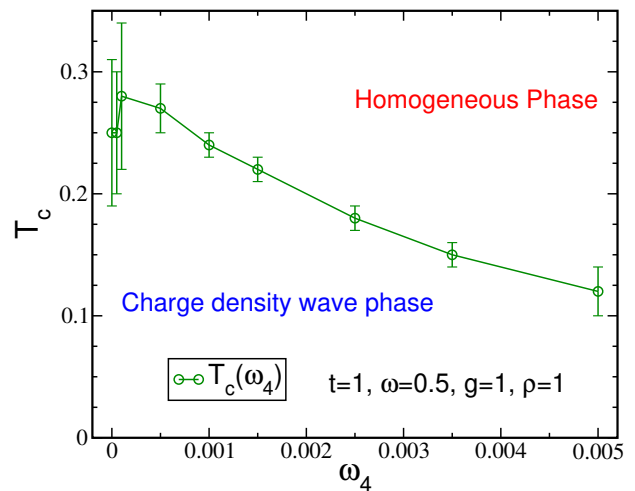


FIG. 8. (Color online). CDW critical temperature, T_c , at half-filling as a function of anharmonicity, ω_4 , for $\omega = 0.5$, $t = 1$, $g = 1$. With sizes up to $L = 12$, the finite size analysis was only feasible for $\omega_4 \leq 0.005$.

model that favors CDW order. The second scenario is the existence of a critical value of ω_4 above which the CDW phase no longer exists.

IV. DOPED SYSTEM

A. First order transition near half-filling

The infinite dimension prediction by Freericks *et. al.*⁴⁰ shows a CDW when the system is doped away from half-filling as well as a SC phase. At sufficiently low temperature, in our Langevin simulations, the evolution of the density with μ , for both $\omega = 0.5$ (Fig. 4) and $\omega = 1$ (Fig. 9), exhibits an abrupt change of the density in the neighborhood of the CDW plateau. We see that these jumps are not finite size effects as their amplitude does not vary much with the size of the system (Fig. 9). We observe this kind of discontinuity in the density for all values of ω_4 , down to $\omega_4 = 0$. They are more pronounced for the lower phonon frequency $\omega = 0.5$. Below half-filling, for $\omega = 1$, the density jumps from $\rho \simeq 0.75$ to $\rho = 1$ and the extent of the jump does not depend much on ω_4 (Fig. 10) although it decreases slightly with increasing ω_4 . We observe a similar jump above half-filling.

For $\omega = 0.5$, the finite temperature effects are stronger and it is more difficult to assess precisely the size of the discontinuity. It appears the change is from $\rho = 1$ to a value which is around $\rho \simeq 0.25$ for $\omega_4 = 0.001$ whereas, as can be observed in Fig. 4, the jump is reduced to $\rho = 1$ down to $\rho \simeq 0.75$ for $\omega_4 = 0.0075$. The structure factor is essentially zero when the density is no longer one. We do not find, at these low temperatures, any sign of an intermediate doped region with nonzero structure factor.

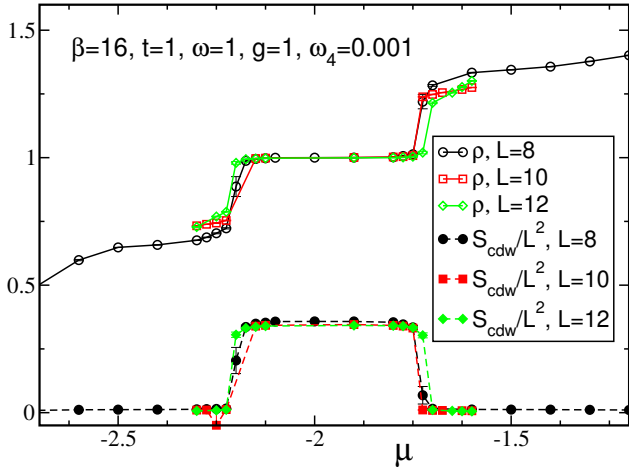


FIG. 9. (Color online). Density, ρ , and structure factor, S_{cdw} , as functions of the chemical potential for $\omega = 1$ and several sizes at $\beta = 16$. An abrupt change of the density is found when the system is doped away from half-filling, which also corresponds to the disappearance of CDW order.

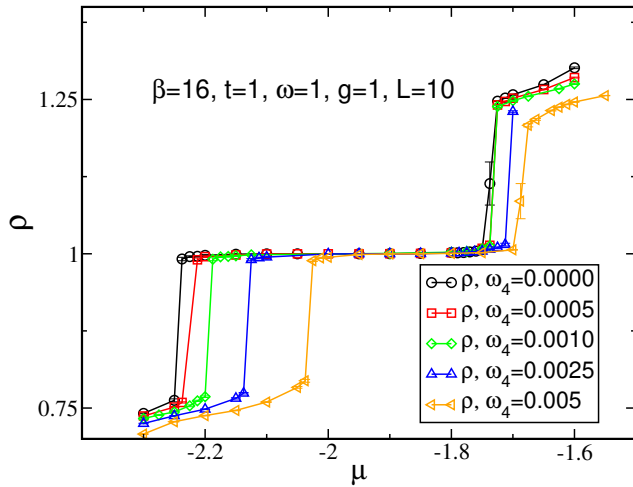


FIG. 10. (Color online). Density, ρ , as a function of the chemical potential for $\omega = 1$ and several values of ω_4 at $\beta = 16$. The abrupt change of the density found when the system is doped is present for all values of ω_4 .

Such discontinuities indicate that the transition, as μ is changed, is of first order. If the simulations were done in the canonical ensemble, there would be phase separation between a CDW and a uniform phase in the jump region, as was observed in bosonic Hubbard models when the system is doped away from a CDW phase.⁵¹ Such a transition was recently observed in variational Monte Carlo simulations²² and was also reported in [52]. To confirm the first order nature of the transition, we analyzed the behavior of the density and energy for a large enough system, $L = 10$, at low temperature, $\beta = 20$, doping below half-filling (Fig. 11). By choosing

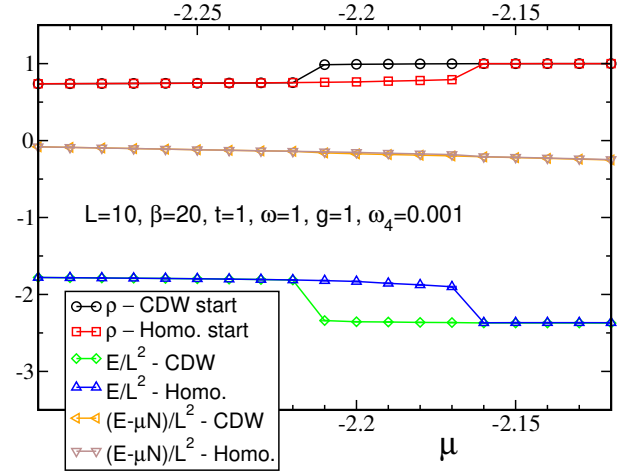


FIG. 11. (Color online). Density, ρ , energy per site, E/L^2 , and grand potential per site, $E/L^2 - \mu\rho$, as functions of μ for different initial conditions of the simulations (CDW start or homogeneous start). We observe hysteresis with an intermediate region where two different phases coexist.

appropriate values of the phonon coordinates, we are able to start the Langevin simulations with two different initial conditions: a homogeneous solution and a CDW one.

For such large systems, the simulations remain “stuck” in the kind of phase that was initially imposed upon the system indicating a metastability characteristic of first order transitions. This leads to hysteresis as is seen clearly in Fig. 11. In the hysteresis region, we find that the grand potentials $E - \mu N$ of the two phases to be essentially equal, and since $E - \mu N$ is minimized at equilibrium, we then observe two equivalent solutions in this chemical potential range. As a consequence, the energy E of the CDW phase is lower than that of the homogeneous phase in the coexistence region.

Contrary to what was observed in infinite dimension,⁴⁰ we do not find in two dimensions a region away from half-filling where CDW order survives. It is noticeable that smaller systems, such as the ones used at the beginning of this study (Fig. 2), or higher temperatures may give the false signal that there is CDW away from half filling because it is possible to choose a value of μ that gives an average density located in the unstable region. The system will then have a broad density distribution ranging from the low homogeneous phase density up to $\rho = 1$, and since measured quantities are averaged over this wide distribution, the structure factor can appear to be nonzero.⁵¹

B. Superconducting behavior

Away from half-filling, the system is expected to become superconducting at low temperatures. However,

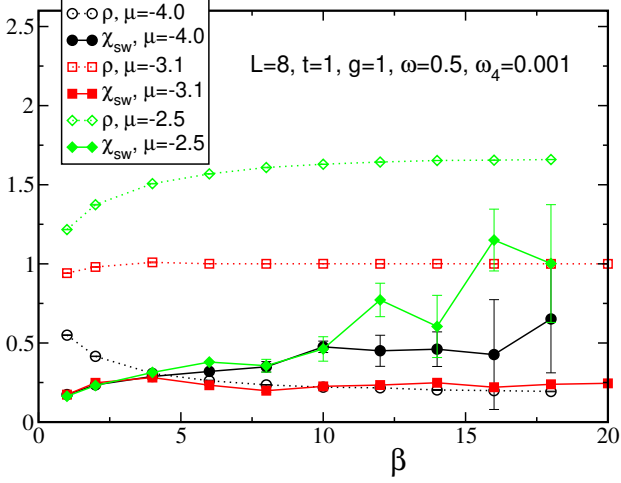


FIG. 12. (Color online). Density, ρ , and s-wave pairing susceptibility, χ_s , as functions of β for $\omega = 0.5$, $\omega_4 = 0.001$, and $g = t = 1$. $\mu = -3.1$ corresponds to the half-filled system, $\mu = -4$ to a lower density $\rho \simeq 0.25$, and $\mu = -2.5$ to $\rho > 1.5$.

in general, the transition temperatures appear to be low.^{31,52} For the $\omega = 1$ harmonic Holstein model, the transition towards a SC state happens for $\beta \simeq 28$ ⁵² and even larger inverse temperature for $\omega = 0.5$. This makes it difficult to observe the effects of anharmonicity on the critical temperature itself, especially since ω_4 is expected to reduce T_c even further. Instead, we will focus on the evolution of the superconducting susceptibility χ_s , without attempting to discern where it might diverge.

Fig. 12 shows the evolution of the density, ρ , as well as the superconducting susceptibility, χ_s , as functions of β for $\omega = 0.5$ and three values of μ corresponding to densities below, at, and above half-filling. We first observe that, away from half-filling, the density reaches its ground state behavior only above $\beta = 10$. As can be expected, the pairing susceptibility at half filling does not diverge, but remains small. For the doped system, it was not possible to observe a divergence of χ_s in the range of accessible temperatures. As shown in Fig. 12, statistical fluctuations in χ_s become large in the doped system for $\beta > 10$, and would become even more problematic in attempting to approach the superconducting transition one expects at much lower temperature.

With this limited access to superconducting behavior, we study the effects of the anharmonicity through the evolution of χ_s as a function of ω_4 for small size and intermediate temperatures $\beta = 8, 10$. In Fig. 13, $\omega = 0.5$, we observe that the superconducting response increases rapidly as ω_4 is increased for a density range $0 < \rho \leq 0.6$. Once again, we observe that increasing ω_4 has roughly the same effect as increasing ω ; it promotes superconductivity. We did not study the region between $\rho = 0.6$ and $\rho = 1$ as it corresponds to the unstable region between homogeneous and CDW phases. We remark

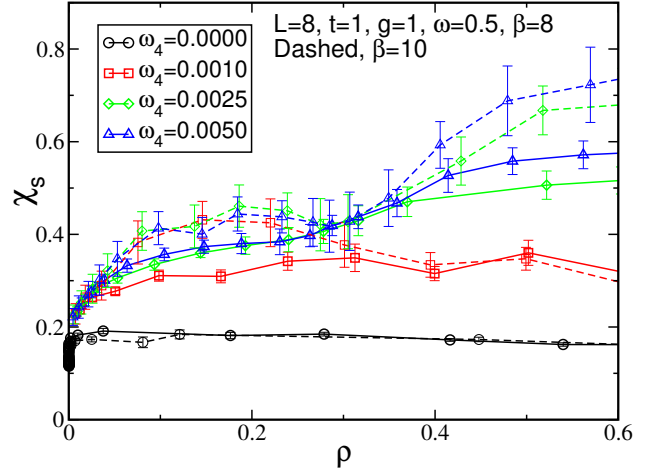


FIG. 13. (Color online). The s-wave pairing susceptibility, χ_s , as a function of density, ρ , for $\omega = 0.5$, $g = t = 1$, different values of ω_4 , and $\beta = 8, 10$. The susceptibility increases as ω_4 or β increases.

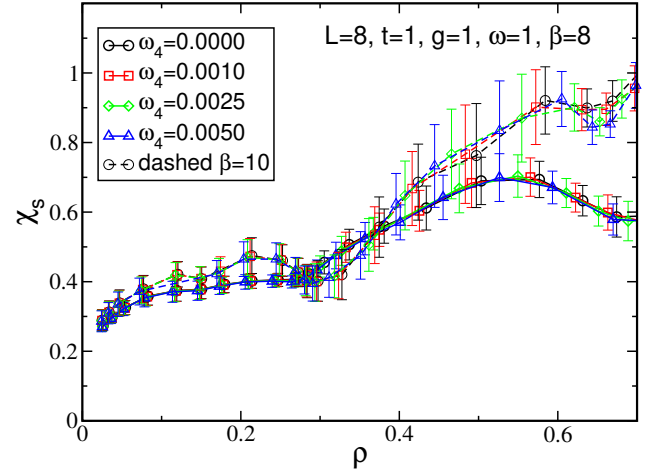


FIG. 14. (Color online). The s-wave pairing susceptibility, χ_s , as a function of density, ρ , for $\omega = 1$, $g = t = 1$, different values of ω_4 , and $\beta = 8, 10$. The susceptibility is not sensitive to changes in ω_4 but increases with β .

that, for the smaller values of ω_4 , the system will already be unstable for $\rho > 0.25$.

For $\omega = 1$, the anharmonicity has limited effect on the SC susceptibility at the values of ω_4 we studied (Fig. 14). This parallels the small ω_4 dependence of the CDW lobe in the phase diagram (Fig. 3(b)) for this phonon frequency.

In both cases, $\omega = 0.5$ (Fig. 13) and $\omega = 1$ (Fig. 14), we observe an increase of χ_s as β goes from 8 to 10 but are not able to observe the divergence of χ_s .

V. CONCLUSIONS

In this work, we studied the effect of an anharmonic quartic term on the physics of the Holstein model at strong electron-phonon coupling, $g = 1$, and phonon frequencies $\omega = 0.5$ and $\omega = 1$. We observed similar effects of the anharmonicity for the two phonon frequencies, but the effects were much reduced for the $\omega = 1$ case in the range of anharmonicities we studied. We found that the main effect of the quartic term is to reduce the importance of the electron-phonon coupling compared to the phonon potential energy. At half-filling, this shrinks the charge gap and leads to a suppression of the CDW structure factor at zero temperature and to a lowering of the critical temperature for the CDW transition.

The behavior of the density as one approaches an insulating plateau has been a central interest in a number of contexts, including early Bethe *ansatz* solutions of the 1D fermion Hubbard model.⁵³ For the 2D fermion Hubbard model, Assaad and Imada used QMC methods to extract critical exponents.⁵⁴ Further fermion work is reviewed in [55]. In parallel, similar issues have been central to the investigation of the boson-Hubbard model, including theoretical prediction⁵⁶ of the mean field nature of the density controlled transition into the Mott lobe which were confirmed by QMC.⁵⁷

In this work, we have added further information to this area by studying the anharmonic Holstein Hamiltonian. Doping the system away from half-filling, we observed a first order phase transition between the CDW phase at half filling and a homogeneous phase at lower densities. This first order transition is present, though not widely studied previously, in the harmonic Holstein model.^{22,52}

In the homogeneous phase below half-filling, for $\omega = 0.5$, we observed a clear enhancement of the superconducting susceptibility at finite temperature as ω_4 is increased. However, with the limited range of accessible temperatures, we were not able to observe the superconducting transition. For $\omega = 1$, ω_4 does not have a strong effect on the superconducting response.

The results we presented here show that the transitions from $\rho = 1$ to $\rho > 1$ and to $\rho < 1$, as μ is tuned, are both first order (Fig. 10). However, most of our results for the doped system focused on $\rho < 1$, and, since the system is no longer particle-hole symmetric, it would be interesting to study its properties above half filling further. To complete the understanding of the role of the quartic term, it is necessary to study the system at other coupling parameters, in particular lower values of g .

ACKNOWLEDGMENTS

We thank Owen Bradley for insights on the superconducting behavior of these systems, and we thank

Steve Johnston and Seher Karakuzu for very useful discussions and comments. This work was supported by the French government, through the UCAJEDI Investments in the Future project managed by the National Research Agency (ANR) with the reference number ANR-15-IDEX-01 and by Beijing Computational Science Research Center. KB acknowledges support from the center of Materials Theory as a part of the Computational Materials Science (CMS) program, funded by the U.S. Department of Energy, Office of Science. The work of RTS was supported by the grant DE-SC0014671 funded by the U.S. Department of Energy, Office of Science. B.C-S acknowledges support from the UC-National Laboratory In-Residence Graduate Fellowship through the UC National Laboratory Fees Research Program.

Appendix A: Approximate values of $\langle x_i \rangle$, μ and U_{eff}

In the harmonic case, the value of the chemical potential at half-filling and of the average phonon displacement can be found exactly by a particle-hole transformation combined with a transformation of the phonon displacement

$$\begin{aligned} c_{i\sigma} &= (-1)^i \tilde{c}_{i\sigma}^\dagger, & c_{i\sigma}^\dagger &= (-1)^i \tilde{c}_{i\sigma}, \\ x_i &= -\tilde{x}_i + x_0, & p_i &= -\tilde{p}_i. \end{aligned} \quad (\text{A1})$$

The transformed Hamiltonian is the same as the original one provided that $x_0 = -2\lambda/\omega^2 = -2\sqrt{2\omega}g/\omega^2$, which cancels out terms that are linear in x_i , and that $\mu = \lambda x_0/2$, which is then the chemical potential at half-filling.

Using this value of μ , the resulting Hamiltonian can be expressed in terms of $\delta_i = x_i - x_0/2$ and is invariant under the particle-hole transformation combined with a $\delta_i \rightarrow -\delta_i$ transformation. This shows that $\langle x_i \rangle$ is exactly equal to $x_0/2 = -\lambda/\omega^2 = -\sqrt{2\omega}g/\omega^2$ in the ground state at half-filling.

We can roughly estimate the relative sizes of the harmonic and anharmonic terms as follows: at half-filling, a CDW phase will develop and we will, approximately, have an alternation of empty and doubly occupied sites. As $\langle x_i \rangle = x_0/2$ when averaged over all sites, the value of x_i on doubly occupied sites can be approximated by x_0 . If we then compute the ratio η of the anharmonic to harmonic terms at x_0 we obtain,

$$\eta \equiv \frac{\omega_4 x_0^4}{\omega^2 x_0^2/2} = \frac{16\omega_4 g^2}{\omega^5} \quad (\text{A2})$$

We can also estimate the effective attraction between fermions. Completing the square of the phonon term at $\omega_4 = 0$ results in

$$\frac{1}{2}\omega^2 x^2 + \lambda x n = \frac{1}{2}\omega^2 \left(x + \frac{\lambda n}{\omega^2} \right)^2 - \frac{\lambda^2}{2\omega^2} n^2 \quad (\text{A3})$$

Since $n^2 = n_\uparrow + n_\downarrow + 2n_\uparrow n_\downarrow$, the second term on the right hand side of this expression gives an attractive

interaction between up and down electrons, $U_{\text{eff}} = -\lambda^2/\omega^2$. The first term shows that the phonon potential energy is indeed minimized at $x_0 = -2\lambda/\omega^2$ on a doubly occupied site.

Adding the anharmonic term (Eq. 1) breaks the particle-hole symmetry and it is no longer possible to derive analytically the value of the chemical potential at half-filling. One can obtain an approximate value by using particle-hole transformation Eq. A1 and by canceling the terms that are linear in x_i , neglecting higher order terms. This leads to the following equation for x_0 :

$$\omega^2 x_0 + 4\omega_4 x_0^3 = -2\lambda \quad (\text{A4})$$

and the chemical potential at half-filling is approximately given by $\mu = \lambda x_0/2$. $|x_0|$ is obviously reduced as ω_4 increases and, then, the chemical potential at half-filling is increased. This approximate formula is used to derive the chemical potential shown in Fig. 3.

Appendix B: Corrections to finite size scaling

For values of ω_4 larger than $\omega_4 = 0.005$ we have not been able, in the range of temperatures and sizes that we could simulate, to find cases where rescaled structure factor curves obtained for different sizes would cross each other. Finite size analysis (Eq. 7) predicts that, for large

systems, $S_{\text{cdw}} \cdot L^{-7/4}$ should take a unique value $\tilde{S}(0)$ at T_c . For $\omega = 0.5$ and $\omega_4 = 0.0075$, we studied system's sizes up to $L = 16$ for $\beta \leq 10$ (see Fig. 15) but, even for these relatively large systems, we could not find a crossing point for the curves and could then not apply a finite size scaling analysis to find the critical temperature.

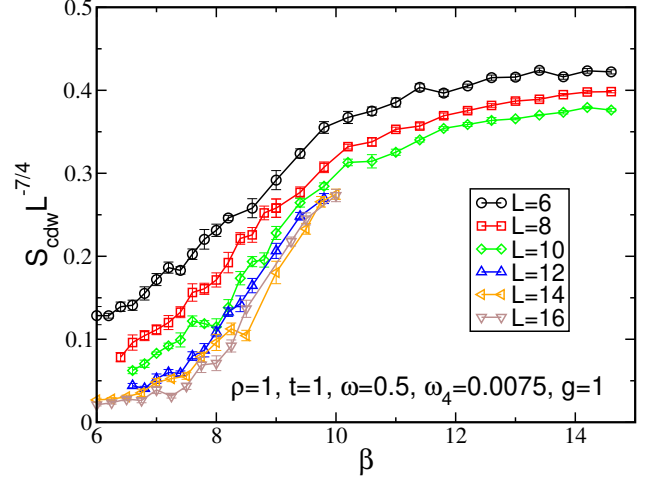


FIG. 15. (Color online). For $\omega_4 = 0.0075$, $\omega = 0.5$ and $L = 6$ to $L = 16$, rescaled data for S_{cdw} do not cross each other, precluding the use of finite size scaling. This is probably due to larger finite size scaling corrections.

* Corresponding author: frederic.hebert@inphyni.cnrs.fr

- ¹ "Electron - Phonon Superconductivity," in *The Physics of Conventional and Unconventional Superconductors*, K.H. Bennemann and J.B. Ketterson, eds., Springer-Verlag (2001).
- ² "Bound Electron Pairs in a Degenerate Fermi Gas," L. N. Cooper, Phys. Rev. **104**, 1189 (1956).
- ³ *Density Waves in Solids*, G. Grüner, Addison-Wesley (1994).
- ⁴ "Electronic crystals: an experimental overview," Pierre Monceau, Adv. in Phys. **61**, 325 (2012).
- ⁵ "The dynamics of charge density waves," G. Grüner, Rev. Mod. Phys. **60**, 1129 (1988).
- ⁶ "Studies of polaron motion: Part I. The molecular-crystal model," T. Holstein, Ann. Phys. **8**, 325 (1959).
- ⁷ "Continuous-Time Quantum Monte Carlo Algorithm for the Lattice Polaron," P.E. Kornilovitch, Phys. Rev. Lett. **81**, 5382 (1998).
- ⁸ "Ground-state dispersion and density of states from path-integral Monte Carlo: Application to the lattice polaron," P.E. Kornilovitch, Phys. Rev. B **60**, 3237 (1999).
- ⁹ "Polaron dynamics and bipolaron condensation in cuprates," A. S. Alexandrov, Phys. Rev. B **61**, 12315 (2000).
- ¹⁰ "Quantum Monte Carlo and variational approaches to the Holstein model," M. Hohenadler, H. G. Evertz, and W. von der Linden, Phys. Rev. B **69**, 024301 (2004).

- ¹¹ "Dimensionality effects on the Holstein polaron," L.-C. Ku, S.A. Trugman, and J. Bonca, Phys. Rev. B **65**, 174306 (2002).
- ¹² "Effect of electron-phonon interaction range on lattice polaron dynamics: A continuous-time quantum Monte Carlo study," P.E. Spencer, J.H. Samson, P.E. Kornilovitch, and A.S. Alexandrov, Phys. Rev. B **71**, 184310 (2005).
- ¹³ "Two dimensional Hubbard-Holstein bipolaron," A. Macridin, G.A. Sawatzky, and M. Jarrell, Phys. Rev. B **69**, 245111 (2004).
- ¹⁴ "Effects of dimensionality and anisotropy on the Holstein polaron," A.H. Romero, D.W. Brown, and K. Lindenberg, Phys. Rev. B **60**, 14080 (1999).
- ¹⁵ "Holstein polaron," J. Bonca, S.A. Trugman, and I. Batistić, Phys. Rev. B **60**, 1633 (1999).
- ¹⁶ R. Peierls, *Surprises in Theoretical Physics*, Princeton University Press (1979).
- ¹⁷ "Effect of Quantum Fluctuations on the Peierls Instability: A Monte Carlo Study," J.E. Hirsch and E. Fradkin, Phys. Rev. Lett. **49**, 402 (1982).
- ¹⁸ "Phase diagram of one-dimensional electron-phonon systems. II. The molecular-crystal model," J.E. Hirsch and E. Fradkin, Phys. Rev. B **27**, 4302 (1983).
- ¹⁹ "Competition of pairing and Peierls-charge-density-wave correlations in a two-dimensional electron-phonon model," R.T. Scalettar, N.E. Bickers, and D.J. Scalapino, Phys. Rev. B **40**, 197 (1989).

- ²⁰ “Holstein model in infinite dimensions,” J. K. Freericks, M. Jarrell, and D. J. Scalapino, *Phys. Rev. B* **48**, 6302 (1993).
- ²¹ “Pairing and charge-density-wave correlations in the Holstein model at half-filling,” F. Marsiglio, *Phys. Rev. B* **42**, 2416 (1990).
- ²² “Competition among Superconducting, Antiferromagnetic, and Charge Orders with Intervention by Phase Separation in the 2D Holstein-Hubbard Model,” T. Ohgoe and M. Imada, *Phys. Rev. Lett.* **119**, 197001 (2017).
- ²³ “Dominant charge density wave correlations in the Holstein model on the half-filled square lattice,” M. Hohenadler and G.G. Batrouni, *Phys. Rev. B* **100**, 165114 (2019).
- ²⁴ “Two-dimensional Holstein-Hubbard model: Critical temperature, Ising universality, and bipolaron liquid,” M. Weber and M. Hohenadler, *Phys. Rev. B* **98**, 085405 (2018).
- ²⁵ “Langevin Simulations of the Half-Filled Cubic Holstein Model,” B. Cohen-Stead, K. Barros, Z.Y. Meng, C. Chen, R.T. Scalettar, and G.G. Batrouni, *Phys. Rev. B* **102**, 161108(R) (2020).
- ²⁶ “Charge Order in the Holstein Model on a Honeycomb Lattice,” Y.X. Zhang, W.T. Chiu, N.C. Costa, G.G. Batrouni, and R.T. Scalettar, *Phys. Rev. Lett.* **122**, 077602 (2019).
- ²⁷ “Interactions between electrons and lattice vibrations in a normal metal,” A.B. Migdal, *Zh. Eksp. Teor. Fiz.* **34**, 1438 (1958); [*Sov. Phys. JETP* **7**, 999 (1958)].
- ²⁸ “Interactions between electrons and lattice vibrations in a superconductor,” G.M. Eliashberg, *Zh. Eksp. Teor. Fiz.* **38**, 966 (1960); [*Sov. Phys. JETP* **11**, 696 (1960)].
- ²⁹ “Quantitative reliability study of the Migdal-Eliashberg theory for strong electron-phonon coupling in superconductors,” Johannes Bauer, Jong E. Han, and Olle Gunnarsson *Phys. Rev. B* **84**, 184531 (2011).
- ³⁰ “Breakdown of the Migdal-Eliashberg theory in the strong-coupling adiabatic regime,” A.S. Alexandrov, *Europhys. Lett.* **56**, 92 (2001).
- ³¹ “Breakdown of the Migdal-Eliashberg theory: A determinant quantum Monte Carlo study,” I. Esterlis, B. Nosarzewski, E. W. Huang, B. Moritz, T. P. Devereaux, D. J. Scalapino, and S. A. Kivelson, *Phys. Rev. B* **97**, 140501(R) (2018).
- ³² “Going beyond the linear approximation in describing electron-phonon coupling: Relevance for the Holstein model,” C. P. J. Adolphs and M. Berciu, *Europhys. Lett.* **102**, 47003 (2013).
- ³³ “The effects of non-linear electron-phonon interactions on superconductivity and charge-density-wave correlations,” Shaozhi Li and S. Johnston, *Europhys. Lett.* **109**, 27007 (2015).
- ³⁴ “Quasiparticle properties of the nonlinear Holstein model at finite doping and temperature,” Shaozhi Li, E.A. Nowadnick, and S. Johnston, *Phys. Rev. B* **92**, 064301 (2015).
- ³⁵ “Relative importance of nonlinear electron-phonon coupling and vertex corrections in the Holstein model,” P.M. Dee, J. Coulter, K. Kleiner, and S. Johnston, *Commun. Phys.* **3**, 145 (2020).
- ³⁶ “Light-enhanced electron-phonon coupling from nonlinear electron-phonon coupling,” M. A. Sentef, *Phys. Rev. B* **95**, 205111 (2017).
- ³⁷ “Phonon-induced disorder in dynamics of optically pumped metals from non-linear electron-phonon coupling,” J. Sous, B. Kloss, D. M. Kennes, D. R. Reichman, and A. J. Millis, arXiv:2009.00619.
- ³⁸ “Polaronic superconductivity in the absence of electron-hole symmetry,” J.E. Hirsch, *Phys. Rev. B* **47**, 5351 (1993).
- ³⁹ “The Hubbard–Holstein Model with Anharmonic Phonons in One Dimension,” Ashok Chatterjee and Yasutami Takada, *J. Phys. Soc. Jap.* **73**, 964 (2004).
- ⁴⁰ “The Anharmonic Electron-Phonon Problem,” J. K. Freericks, Mark Jarrell, and G. D. Mahan, *Phys. Rev. Lett.* **77**, 4588 (1996).
- ⁴¹ “Metallicity in a Holstein-Hubbard Chain at Half Filling with Gaussian Anharmonicity,” Ch. Uma Lavanya, I. V. Sankar, and Ashok Chatterjee, *Sci. Rep.* **7**, 3774 (2017).
- ⁴² “Effect of lattice anharmonicity on superconductivity,” J.C.K. Hui and P. B. Allen, *J. Phys. F* **4**, L42 (1974).
- ⁴³ “Influence of Anharmonicity on Superconductivity,” A.E. Kavakozov and E.G. Maksimov, *Zh. Eksp. Teor. Fiz.* **74**, 681 (1978); [*Sov. Phys. JETP* **47**, 358 (1978)].
- ⁴⁴ “Resistivity and superconductivity from anharmonic phonons,” G.D. Mahan and J.O. Sofo, *Phys. Rev. B* **47**, 8050 (1993).
- ⁴⁵ “Langevin simulations of a long-range electron-phonon model,” G.G. Batrouni and R.T. Scalettar, *Phys. Rev. B* **99**, 035114 (2019).
- ⁴⁶ “Langevin simulations of lattice field theories,” G. G. Batrouni, G. R. Katz, A. S. Kronfeld, G. P. Lepage, B. Svetitsky, and K. G. Wilson, *Phys. Rev. D* **32**, 2736 (1985).
- ⁴⁷ “Monte Carlo calculations of coupled boson-fermion systems. I,” R. Blankenbecler, D.J. Scalapino, and R.L. Sugar, *Phys. Rev. D* **24**, 2278 (1981).
- ⁴⁸ *Quantum Monte Carlo Methods: Algorithms for Lattice Models*, by J. Gubernatis, N. Kawashima, and P. Werner, Cambridge University Press (2016).
- ⁴⁹ “Phonon Dispersion and the Competition between Pairing and Charge Order,” N.C. Costa, T. Blommel, W.-T. Chiu, G. Batrouni, and R. T. Scalettar, *Phys. Rev. Lett.* **120**, 187003 (2018).
- ⁵⁰ “Principal component analysis for fermionic critical points,” N. C. Costa, W. Hu, Z. J. Bai, R. T. Scalettar, and R. R. P. Singh, *Phys. Rev. B* **96**, 195138 (2017).
- ⁵¹ “Phase Separation in Supersolids,” G. G. Batrouni and R. T. Scalettar *Phys. Rev. Lett.* **84**, 1599 (2000).
- ⁵² “Superconductivity and charge density wave order in the 2D Holstein model,” O. Bradley, G.G. Batrouni, and R.T. Scalettar, arXiv:2011.11703.
- ⁵³ “Critical exponents for the one-dimensional Hubbard model,” H. Frahm and V.E. Koropin, *Phys. Rev. B* **42**, 10553 (1990).
- ⁵⁴ “Insulator-Metal Transition in the One- and Two-Dimensional Hubbard Models,” F. F. Assaad and M. Imada, *Phys. Rev. Lett.* **76**, 3176 (1996).
- ⁵⁵ “Metal-insulator transitions,” M. Imada, A. Fujimori, and Y. Tokura, *Rev. Mod. Phys.* **70**, 1039 (1998).
- ⁵⁶ “Boson localization and the superfluid-insulator transition,” M.P.A. Fisher, P.B. Weichman, G. Grinstein, and D.S. Fisher *Phys. Rev. B* **40**, 546 (1989).
- ⁵⁷ “Quantum Critical Phenomena in one-dimensional Bose Systems,” G.G. Batrouni, R.T. Scalettar, and G.T. Zimanyi, *Phys. Rev. Lett.* **65**, 1765 (1990).